RSC Advances

PAPER

View Article Online
View Journal | View Issue

Cite this: *RSC Adv.*, 2025, **15**, 30969

A highly sensitive label-free aptamer sensor for timely detection of human serum albumin

Hanghang Cheng,[ab] Wentao Chen,[ab] Zejun Deng,[c] Minghui Yin,[ab] Chengyu Zhuang,*[d] Zhi-mei Qi,*[ab] Ning Xue*[e] and Chunxiu Liu*[ab]

The trace-level detection of proteins in the human body holds significant importance for health monitoring and disease prevention. To conduct real-time monitoring of the human body's health status, both wearable and implantable devices require label-free sensing. However, the signals of a considerable number of label-free electrochemical sensors originate from the signal capture medium. These signals are weak and are prone to being lost or masked by other signals. We report a Prussian blue (PB)-based self-redox aptamer sensor was developed, enabling real-time human serum albumin (HSA) detection without external redox mediators. The designed sensing interface successfully achieved the quantitative detection of HSA in PBS with a sensitivity of 124 fg mL^{-1}. In addition, to validate universality, the sensor was tested with retinol-binding protein (RBP4), showing comparable performance. This label-free electrochemical sensor can achieve one-step detection without additional reagents. This system has application potential in on-site detection, as well as wearable sensing.

Received 21st July 2025
Accepted 21st August 2025

DOI: 10.1039/d5ra05254h

rsc.li/rsc-advances

1 Introduction

Immunoanalysis is gradually becoming the most popular platform in clinical testing and biosensors.[1–3] Immunological techniques selectively respond to specific biological targets by capturing the specific interaction between probe and target. Various mechanisms for detecting target biomolecules have been developed and studied based on immunorecognition. These can be divided into mechanical,[4] optical,[5] electrochemical,[6–8] and colorimetric[9,10] methods according to the response mechanisms.

HSA, synthesized and secreted by the liver, is the most abundant protein in the circulatory system. Decreased HSA concentration usually accompanies the occurrence of liver disease.[11] Quantitative detection is crucial for assessing liver function and the human circulatory system. Mechanisms for detecting HSA include mechanical,[12] optical,[11,13] and electrochemical[14,15] methods. Previous wearable sensing systems were limited to analyzing substances within the micro-molar to millimolar range.[16] However, since the content of HSA in sweat is small and there are many interferents, a sensor suitable for non-invasive, rapid, and sensitive detection is required.

Electrochemical immunosensors have received extensive attention due to their portability, good performance, simplicity of equipment, and low cost.[17] Selecting appropriate immunorecognition substances is also crucial. Replacing antibodies with aptamers in immunoanalysis has been widely investigated, as aptamers have few limitations on target substances and can be used to detect a variety of substances, with advantages such as small molecular weight, rapid amplification, and simple quality control.[18] Gold nanoparticles (AuNPs) are considered the most popular nanomaterials for developing aptamer sensors due to their physical and chemical properties.[19,20] The binding of AuNPs in electrochemical aptamer sensors has the potential to amplify electrochemical signals based on AuNPs performance, and decorating AuNPs on electrode surfaces can significantly enhance their electrochemical activity.

In previous studies, the signal generation layer of aptamer electrochemical sensors was often fixed at the end of the aptamer, and the electrical signal change was generated through the conformational change of the aptamer after binding to the target. To solve the problems of signal loss and poor signal quality, this study proposes an electrochemical deposition signal layer to detect the target substance. Firstly, PB was modified on the surface of the glassy carbon electrode by cyclic voltammetry (CV) method as an electrical signal generation layer. After that, AuNPs were deposited on stereoscopic screen-printed carbon electrodes using an electrochemical deposition method.[21] Then, the activated aptamer was chemically bound to AuNPs through disulfide bonds. Finally, 6-mercaptohexanol (MCH) was used to close the remaining sites on the AuNPs surface,[22] reducing non-specific adsorption and

[a]*State Key Laboratory of Transducer Technology, Aerospace Information Research Institute (AIR), Chinese Academy of Sciences, Beijing, China. E-mail: zhimei-qi@mail.ie.ac.cn; cxliu@mail.ie.ac.cn*

[b]*University of Chinese Academy of Sciences, Beijing, China*

[c]*Central South University, Changsha, China*

[d]*Ruijin Hospital, Shanghai Jiao Tong University School of Medicine, Shanghai, China. E-mail: zhuangchengyu@msn.com*

[e]*Lingang Laboratory, Shanghai, China. E-mail: xuening@mail.ie.ac.cn*

obtaining easily prepared and highly sensitive sensor electrode materials. The method's universality was validated using RBP4 protein. After electrode preparation, SEM, EDS and other techniques were used to characterize the electrode surface, differential pulse voltammetry (DPV) and square wave voltammetry (SWV) were primarily used to detect HSA to evaluate the performance of the sensing materials.

2 Materials and methods

2.1 Reagents and instruments

Ferric chloride ($FeCl_3$, 98%, Shanghai Aladdin Biochemical Technology Co., Ltd), potassium ferricyanide ($K_3[Fe(CN)_6]$, ≥99.5%, Shanghai Aladdin), potassium ferrocyanide ($K_4[Fe(CN)_6]$, ≥99.5%, Shanghai Aladdin), potassium chloride (KCl, AR, Sinopharm Chemical Reagent Co., Ltd), chloroauric acid (AR, Aladdin), hydrochloric acid (HCl, AR, Beijing Chemical Works), 6-mercapto-1-hexanol (98%, Aladdin), Tris–EDTA buffer (TE buffer, AR, Beijing Wokai Biotechnology Co., Ltd), tris(2-carboxyethyl)phosphine (TCEP, AR, Shanghai Macklin Biochemical Co., Ltd), phosphate buffered saline (PBS tablets, Shanghai Solarbio Technology Co., Ltd), interleukin-6 (IL-6, AR, Beijing Borui De Biotech Co., Ltd), human serum albumin (HSA, Recombinant, AR, Anbaishun Diagnostics Co., Ltd), retinol-binding protein 4 (RBP4, AR, Shanghai Yubo Biotechnology Co., Ltd).

Electrochemical workstation CHI760E, Shanghai Chenhua Instrument Co., Ltd. Magnetic stirrer MS7-H550-Pro, Jiangsu Jinyi Instrument Technology Co., Ltd. Electronic analytical balance FA2004N/0.1 mg, Bangyi Precision Measuring Instrument (Shanghai) Co., Ltd. Scanning electron microscope S-4800, Hitachi, Japan.

2.2 Electrode preparation process

The flexible electrode used in the experiment was prepared by screen printing conductive carbon ink on a polyimide flexible substrate (produced by Shanghai Chen Hua Instrument Co., Ltd). Carbon is printed on a flexible substrate as the base material for the working electrode and the counter electrode to obtain a glassy carbon electrode (GCE) and Ag/AgCl was printed as the reference electrode. A schematic diagram of the electrode is shown in Fig. 1. In the experiment, the functionalization of the electrode was performed on the working electrode. The specific steps are shown in Fig. 1a.

2.3 Deposition of Prussian blue

In order to detect electrical signals originating from the electrode itself, substances with inherent redox properties are

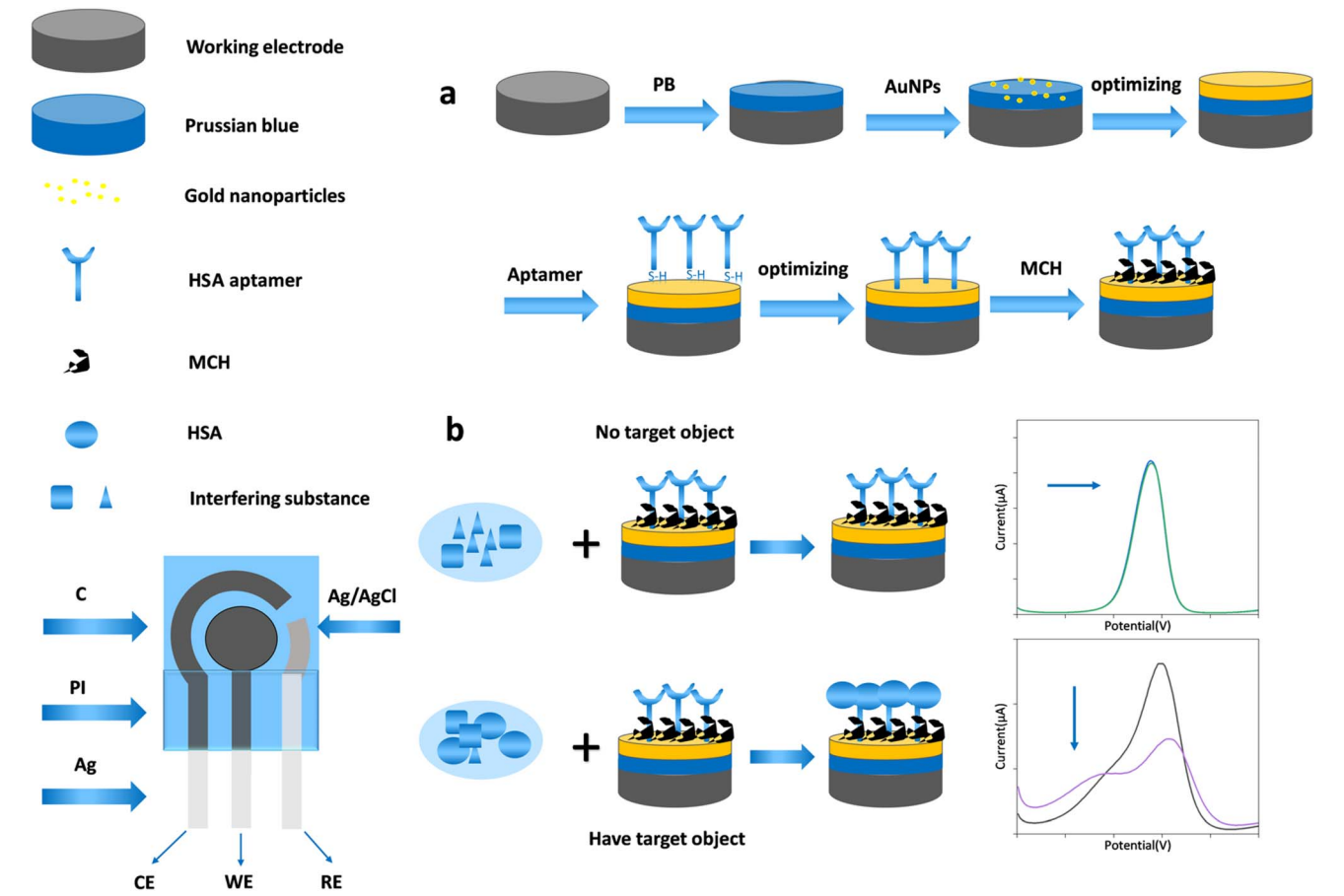

Fig. 1 Electrode schematic. (a) Electrode modification steps. (b) Electrode working principle.

chosen to be modified onto the electrode. Prussian blue[23] (PB) is a substance with redox properties commonly used in experiments. The preparation methods of PB mainly include electrodeposition, chemical assembly, hydrothermal synthesis, and microwave synthesis. Through electrodeposition,[24] researchers have deposited PB on various substrates such as carbon electrodes, tin-oxide steel, and carbon nanotubes to synthesize composite materials with specific properties. First, CV is used to deposit PB on a carbon-based electrode, and the preparation of the electrolyte consists of 5 mM potassium ferrocyanide and 1 : 1 ferric chloride (including 0.13 M hydrochloric acid solution and 5 mM potassium chloride). Then the electrode is immersed in the above electrolyte, and a continuous scan of 20 cycles is performed at a potential range of −0.2 V to 0.9 V using a three-electrode system (with a carbon electrode as the working electrode, an Ag/AgCl electrode as the reference electrode, and a platinum wire electrode as the counter electrode).[25]

2.4 Deposition of gold nanoparticles

We used a simple and rapid constant potential electrochemical deposition method to deposit AuNPs on electrodes.[26] Perform potentiostatic deposition at −0.3 V for 100 s in 1 mM chloroauric acid ($HAuCl_4$). The $HAuCl_4$ solution was continuously stirred using a magnetic stirrer equipped with a stirring bar (stirring speed: 200 rpm). After deposition, the electrode was rinsed thoroughly with deionized water and soaked in deionized water for 10 minutes to remove residual $HAuCl_4$. Finally, the electrode was dried with a rubber bulb syringe and stored in a clean Petri dish for subsequent use.

2.5 Assembly of specific recognition molecules

The HSA-binding ssDNA aptamer used in this study was purchased from Biological Engineering (Shanghai Co., Ltd). The selection of aptamers was rigorously guided by a comprehensive literature review synthesizing findings from prior investigations on these molecules.[27] The HSA-binding aptamer consists of 23 bases and has been modified on both ends with an amine group on the 5′ and a thiol group on the 3′(5′Amino C6/TGCGGTTGTAGTACTCGTGGCCG/Thiol C6 SS 3′).[28] The lyophilized aptamer powder was initially reconstituted in Tris–EDTA (TE) buffer to prepare a 100 μM stock solution.[29] To prevent thiol group cross-linking, the aptamer was treated with 100 mM tris(2-carboxyethyl)phosphine (TCEP) to reduce disulfide bonds.[30] The solution was diluted to 10 μM with TE buffer and stored at 4 °C. Aptamer solution was dropped onto the electrode modified with AuNPs, and reacted at 4 °C for 7 hours. To passivate residual active sites on the AuNPs, 20 μL of 1 mM MCH solution was applied to the working electrode and incubated at room temperature for 1.5 hours. Excess MCH was rinsed off with deionized water, and the electrode was dried and stored at 4 °C for subsequent use.[31] The sensing interface of MCH/aptamer-SH/AuNPs/PB/GCE was obtained.

2.6 Electrochemical measurements

Cyclic voltammetry (CV) measurements were per formed in PBS with the parameters set as follows: step potential, 4 mV; amplitude, 50 mV; and potential range, −0.4 to 0.6 V. Electrochemical impedance spectroscopy (EIS) tests were conducted in a mixed solution containing 0.1 M KCl and 5 mM $K_3[Fe(CN)_6]$/$K_4[Fe(CN)_6]$ (1 : 1) with AC voltage amplitude set as 5 mV, scanning frequency ranged from 0.1 Hz to 100 kHz. Differential pulse voltammetry (DPV) tests were conducted in a solution containing 20 mM $K_3[Fe(CN)_6]$ with voltage amplitude set as 50 mV, potential ranges from −0.4 V to 0.6 V, pulse width is 0.06 s, potential increment is 4 mV, sampling width is 0.02 s, and the pulse period is 0.5 s. Square wave voltammetry (SWV) detection is carried out in PBS, and the parameter settings are as follows: potential ranges from −0.4 V to 0.4 V, frequency is 30 Hz, step potential is 4 mV, and amplitude is 25 mV. Error bars shown in the figures signify standard deviation of three-times parallel measurements.

2.7 Experimental principle

In the presence of the target analyte, the surface-immobilized aptamers undergo specific binding with target molecules, inducing enhanced steric hindrance at the electrode interface. This interfacial modification manifests as a measurable decrease in the faradaic current during electrochemical detection. Conversely, in the absence of the target, the electrode surface remains largely unperturbed, resulting in negligible current variation. Schematic diagram of the working principle is shown in Fig. 1b.

3 Results and discussion

3.1 SEM and EDS imaging of immunosensor surface

Scanning electron microscopy (SEM) was employed for morphological characterization. As shown in the left side of Fig. 2a, the carbon electrode surface exhibits distinct grooves and plateaus, providing favorable nucleation sites for subsequent AuNPs electrodeposition. The left side of Fig. 2b displays a high-resolution SEM image of AuNPs-modified electrodes, revealing cluster-deposited AuNPs with an average diameter of approximately 100 nm. Fig. 2c shows the modification of gold nanoparticles on the Prussian blue substrate on the left side.

Energy-dispersive X-ray spectroscopy (EDS) analysis was conducted to verify elemental composition. The pristine carbon electrode spectrum (right side of Fig. 2a) shows dominant C and O peaks, where the oxygen signal originates from the acrylic acid binder. After depositing gold nanoparticles, the EDS mapping (right side of Fig. 2b) confirmed the existence of the characteristic peak of Au, aligning with SEM-observed nanoparticles. The characteristic peaks of iron and gold appearing in the EDS on the right side of Fig. 2 indicate that both Prussian blue and gold nanoparticles have been successfully modified.

3.2 Detection of HSA

The sensor has a PB signal layer formed by electrochemical deposition and can perform label-free sensing detection. When depositing PB on the carbon electrode and starting to deposit gold nanoparticles, it can be obtained that the electrodeposition of AuNPs may lead to an increase or decrease in the signal,

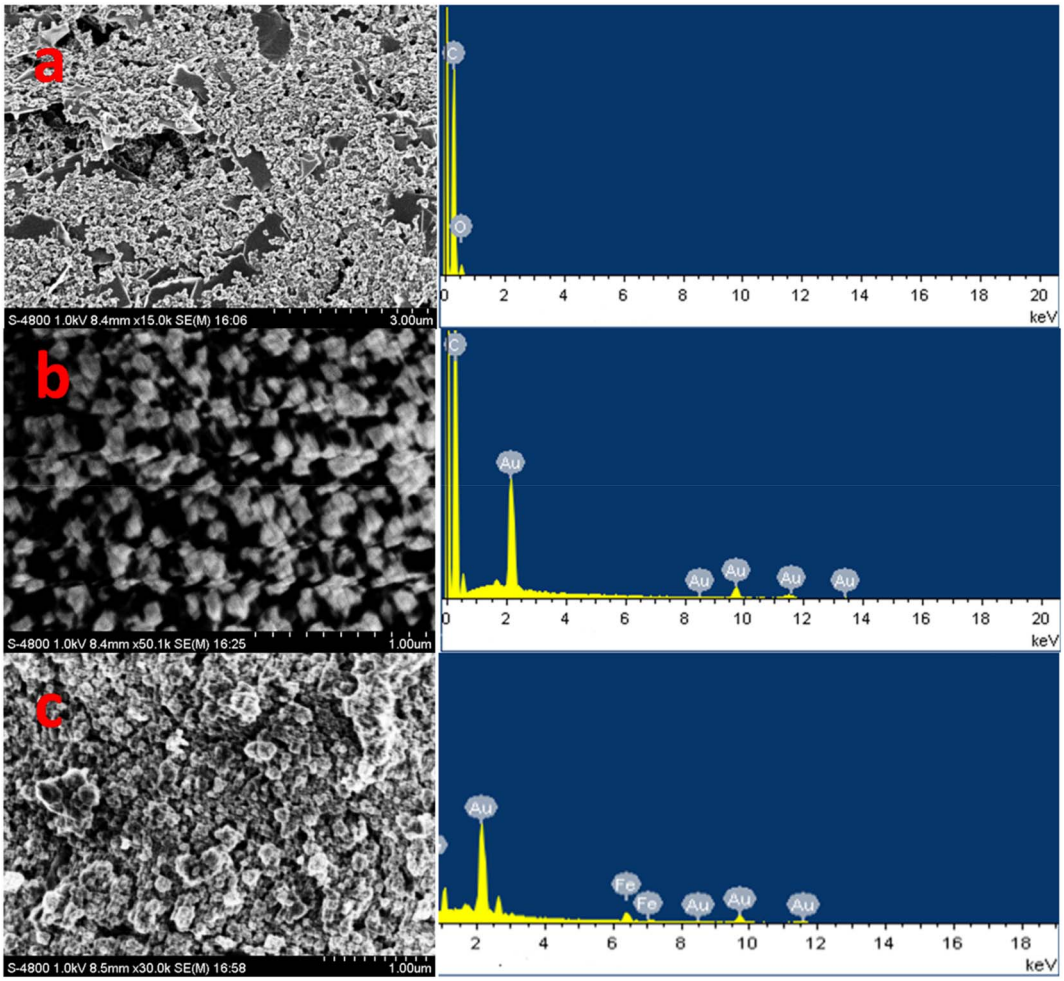

Fig. 2 Electrode structure and morphology characterization. (a) SEM and EDS image of carbon electrode. (b) SEM and EDS image of electrodepositing gold electrode. (c) SEM and EDS image of electrode modified with gold nanoparticles on Prussian blue substrate.

and the electrochemical signal can be enhanced when the electrodeposition time is relatively short (within 60 seconds) due to the stronger conductivity of AuNPs. As the electrodeposition time increases further, AuNPs gradually cover PB, resulting in a decreasing signal in PBS. The results are shown in Fig. 3c. However, a higher signal is not always better. Considering that the aptamer for specific recognition of the target substance is modified on AuNPs the content of AuNPs is also very important. After considering, it was decided to electrodeposit for 100 s to maintain a high signal while having enough AuNPs for aptamer modification. After modification with AuNPs, perform aptamer and MCH modification.

After preparing the HSA aptamer sensor, SWV is used to electrochemically detect HSA to characterize the sensor performance, and the detection solution is PBS. First, different concentrations of HSA solutions are prepared, including 0.1 pg mL^{-1}, 1 pg mL^{-1}, 10 pg mL^{-1}, 100 pg mL^{-1}, 1 ng mL^{-1}, and 10 ng mL^{-1}, dissolved in PBS. Then, the test starts from low concentration to high concentration. 20 μL of a certain concentration of HSA solution (transferred in order from low to high concentration) is transferred to the surface of the prepared working electrode, and the reaction is combined for 30 minutes. Afterward, the remaining HSA solution is slowly washed off with deionized water, and the working electrode is dried with a rubber bulb syringe. SWV detection is performed in PBS and the electrochemical signal is recorded. From Fig. 3a and b, it can be seen that as the concentration of HSA increases from 0.1 pg mL^{-1} to 100 pg mL^{-1}, the SWV peak current decreases, and the electrochemical signal value shows a linear relationship with the logarithm of the HSA concentration, $I = 103.7 - 21.2 \log C$, where I is in μA and C is in g mL^{-1}. The limit of detection (LOD) is 124 fg mL^{-1} based on a signal-to-noise ratio (S/N) of 3. Table 1 lists the detection limits of different detection methods for HSA and the detection limits of the same aptamer electrochemical sensor for other molecules. This indicates that the Prussian blue-based aptamer sensor electrode has been successfully prepared, and the sensor has good sensitivity. The detection range is wide possibly because PB itself also has a signal amplification effect, which can recognize subtle changes on the electrode surface.

Then, the influence of the electrode storage time on the electrode stability was explored. Fig. 3d is the SWV current peak diagram of the Prussian blue-based albumin aptamer sensor after being continuously placed for 0, 1, 2, and 3 days (4 °C)

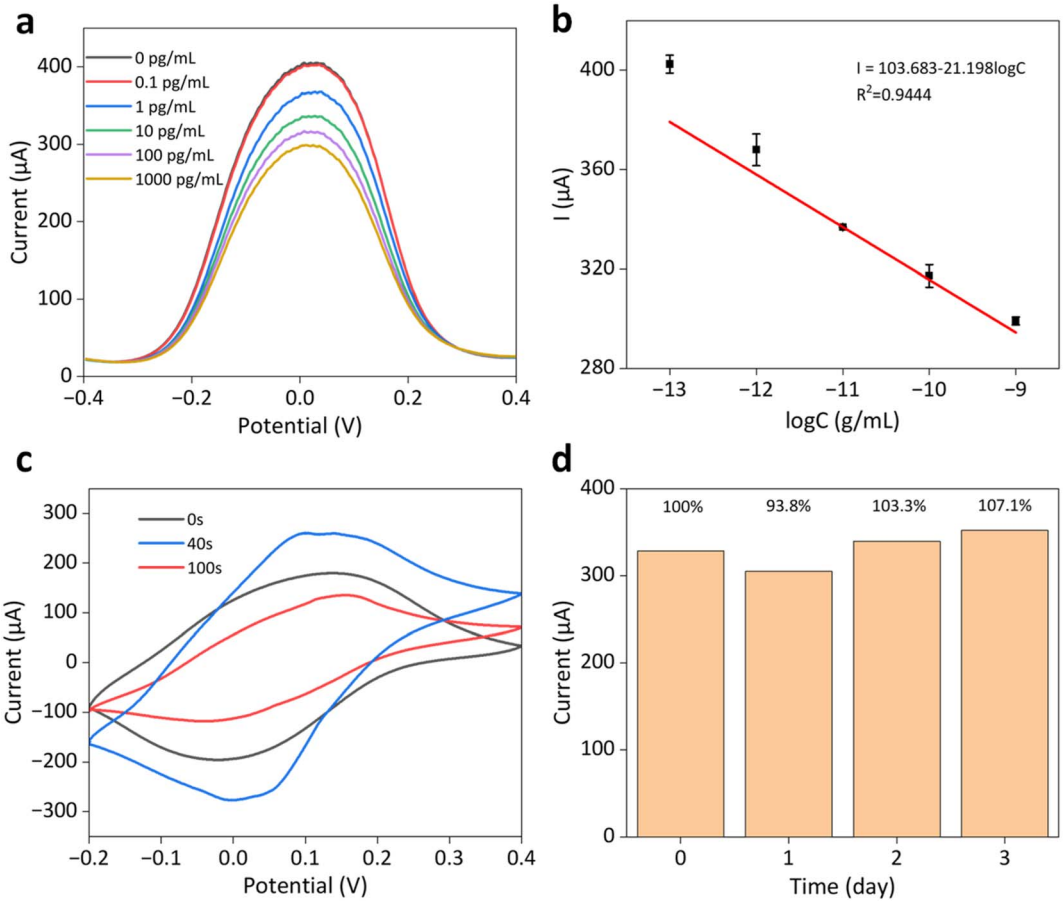

Fig. 3 The Prussian blue-based aptamer sensor sensitivity testing data graph for HSA. (a) SWV curve graph detected at different HSA concentrations. (b) Relationship graph between SWV peak current after data processing and HSA concentration. (c) The influence of electrochemical deposition time on CV electrical signal. (d) The stability of the SWV peak current of the Prussian blue-based aptamer sensor.

respectively. It can be seen that the current decreased by 6.2% after 1 day, increased by 3.3% after 2 days, and increased by 7.1% after 3 days. The relative error of the current signal of the Prussian blue-based aptamer sensor within 3 days is less than 10%, indicating that the prepared sensor also has good stability.

3.3 Sensor functional verification

3.3.1 Electrochemical method confirms surface modification. In order to conduct a feasibility analysis of the sensor and optimize its functional parameters, electrodes without a deposited PB signal layer were used for functional verification. In this step, potassium ferricyanide served as the redox probe for characterizing electrode modification efficacy *via* cyclic voltammetry (CV) and electrochemical impedance spectroscopy (EIS). Following aptamer immobilization (10 μM, 4 °C for 5 h), the AuNPs-modified electrode exhibited significantly increased charge transfer resistance (R_{ct}, evidenced by expanded semicircle diameter in Nyquist plots[39]) and attenuated CV peak currents with positive potential shifts (Fig. 4a). These observations confirm successful aptamer grafting onto AuNPs through

Table 1 Comparison of sensor sensitivity

Detect substances	Detection limit	Method	Reference	Signal sources	Solution	Label required
HSA	32 ng mL^{-1}	Photoluminescence	11	—	—	—
HSA	39 ng mL^{-1}	Magnetoelastic	12	—	—	—
HSA	20 mg mL^{-1}	Electrochemical	32	$[Fe(CN)_6]^{3-/4-}$	$[Fe(CN)_6]^{3-/4-}$	Yes
HSA	865 ng mL^{-1}	Electrochemical	33	$[Fe(CN)_6]^{3-/4-}$	$[Fe(CN)_6]^{3-/4-}$	Yes
HSA	2.6 ng mL^{-1}	Electrochemical	34	$[Fe(CN)_6]^{3-/4-}$	$[Fe(CN)_6]^{3-/4-}$	Yes
HSA	124 fg mL^{-1}	Electrochemical	This work	PB	PBS	No
TNF-α	5 pg mL^{-1}	Electrochemical	35	Fc for aptamer	Tris buffer	No
Insulin	20 nM	Electrochemical	36	MB for aptamer	Tris buffer	No
Immunoglobulin E	60 pM	Electrochemical	37	MB for aptamer	Human serum	No
Thrombin	360 nM	Electrochemical	38	MB for aptamer	Tris buffer	No

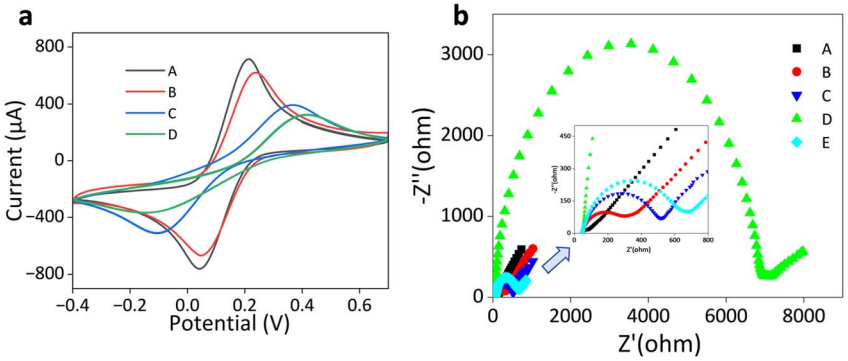

Fig. 4 Cyclic voltammogram and Nyquist plot. (a) A, B, C, D represent electrodeposition of AuNPs, adapter modification, MCH blocking, and carbon electrode, respectively. (b) A, B, C, D, E represent electrodeposition of AuNPs, adapter modification, MCH blocking, carbon electrode, and sealed electrode with addition of 1 ng per mL HSA. The inset shows an enlarged view near the origin in plot.

thiol–gold covalent binding, which introduces steric hindrance and reduces interfacial electron transfer efficiency due to the non-conductive nature of DNA strands.

Subsequent treatment with MCH for 1 hour further elevated R_{ct} and diminished CV currents (Fig. 4b, B *vs.* C), attributable to MCH passivation of residual AuNPs surface sites, thereby amplifying electron transfer blocking effects. Post-target recognition, the impedance shift (Fig. 4b, C *vs.* E) validates both the biorecognition capability of immobilized aptamers and the feasibility of this surface functionalization strategy.

From the CV and EIS characterization, it can be known that the experimental steps and plan are feasible, and each step successfully modified the electrode surface.

3.3.2 Electrochemical optimization of the immunosensor. Electrodeposition of AuNPs was carried out in 1 mM gold chloride solution, the experimental potentials were −0.2 V, −0.3 V, −0.4 V, −0.5 V, −0.6 V, and −0.8 V. Electrodeposition was carried out for the same time (400 s) under each potential, and characterized using CV method. The optimal deposition condition corresponds to the highest peak current, indicating the strongest signal enhancement effect of AuNPs. From Fig. 5a and b, it can be seen that under the same electrodeposition time of 400 s, the CV peak is the highest when the deposition potential is −0.3 V. Subsequently, the electrodeposition time was optimized (Fig. 5c), and carbon electrode was electrodeposited for 300 s, 400 s, 500 s, and 600 s under −0.3 V. It was

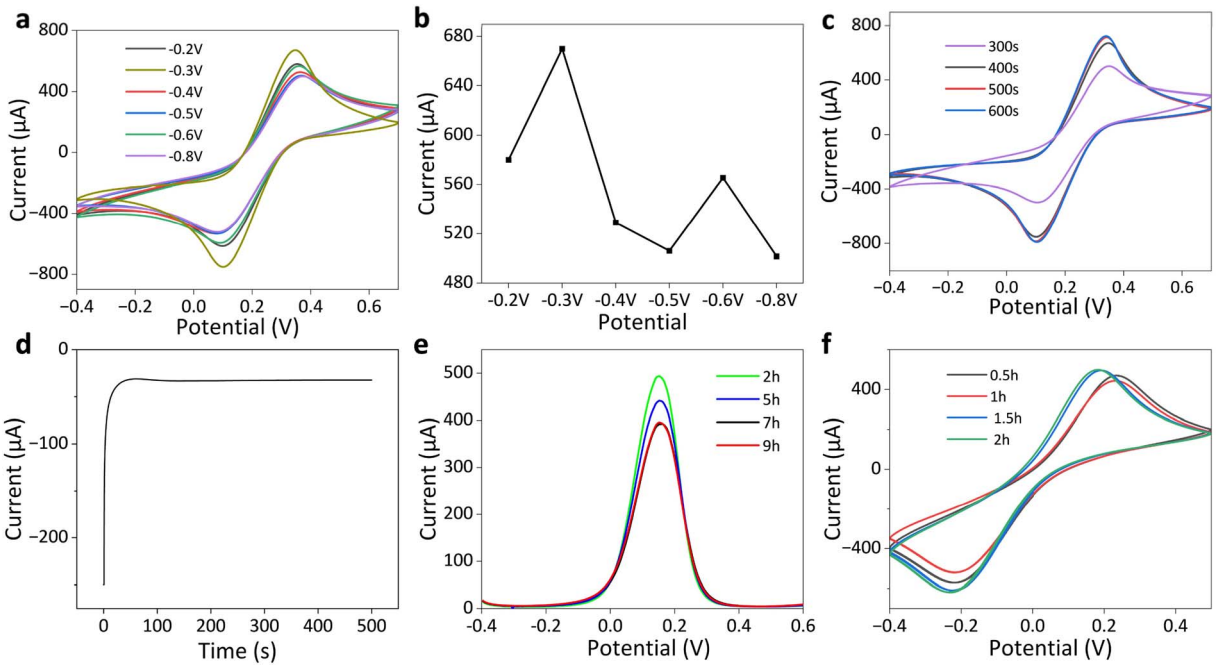

Fig. 5 Optimization of experimental conditions for electrode functionalization. (a) CV plot of electrodeposition at different potentials for 400 s. (b) Peak current values in CV at different potentials. (c) CV plots at different deposition times at −0.3 V deposition potential. (d) *i*–*t* plot of deposition for 500 s at −0.3 V potential. (e) DPV signal after binding of ligand solution to electrode for different durations. (f) CV curves after MCH blocking for different durations.

found that the signal continuously increased between 300 s and 500 s, but decreased at 600 s. This might be due to the fact that the volume and number of AuNPs reached their optimal state at 500 seconds, and as time went on, the nanoparticles further grew, resulting in a decrease in specific surface area and signal size. Therefore, the experimental condition for electrodepositing AuNPs was selected as electrodeposition for 500 s at a constant potential of −0.3 V.

The binding degree of aptamer and AuNPs on the electrode affects the sensitivity of target molecule detection signal, which is influenced by the aptamer concentration and the modification time of aptamer on the electrode. Therefore, the modification time of aptamer was optimized in this experiment, and the influence of different binding times on the DPV peak current of aptamer electrochemical sensor at aptamer concentration of 10 μM was studied. Under the optimal electrodeposition conditions, 20 μL of 10 μM aptamer solution was transferred to the working electrode with a pipette, and the working electrode surface was covered with a centrifuge tube and placed at 4 °C for reaction. The reaction was carried out for 2 hours, 5 hours, 7 hours, and 9 hours, and then the electrode surface was rinsed with deionized water and dried with a rubber bulb syringe. DPV testing was then performed. It can be seen from the Fig. 5e that before the reaction time of 7 hours, the signal continued to decrease, indicating that the aptamer continued to bind to the electrode, and more and more aptamer was bound to the AuNPs through thiol groups, affecting electron transfer and leading to a continuous decrease in signal. However, after 7 hours of reaction, since the aptamer modification had reached saturation, most of the aptamer modification sites were occupied. Therefore, the optimal time for aptamer modification is 7 hours, and this will be used as the best reaction time for further research.

After aptamer modification, since the AuNPs on the electrode were not completely blocked, there will still be a certain degree of non-specific adsorption. To reduce the non-specific adsorption of the electrode, MCH is used to block the remaining active sites on the AuNPs, and the sealing time is closely related to the sealing effect. Evaluating the sealing effect is similar to aptamer modification: when the MCH binding to the AuNPs reaches saturation, it maximizes the impedance of electron transfer to the electrode, showing the lowest signal. Due to the irritating smell of MCH, a 1 mM solution is used for sealing, and the operation is carried out in a fume hood. The sealing time is varied from 0.5 h, 1 h, 1.5 h, to 2 h. CV tests are performed on the electrode signal after sealing, and the final CV results are shown in Fig. 5f. The lowest electrode signal is obtained when the sealing time is 1.5 h, indicating the best sealing effect. Therefore, 1.5 h is selected as the optimal sealing time.

3.4 Portable circuit design and sensing system

To enhance the portability of this protein sensor and adapt it to daily life application scenarios, this study developed an integrated circuit system for interleukin-6 (IL-6) detection. To achieve the integration of the electrode and PCB, we 3D-printed a housing that is compatible with both the electrode and the circuit board. The IL-6-binding aptamer has been modified on both ends with an amine group on the 5′ and a thiol group on the 3′(5′Amino C6/CTTCCACGCTCGTATTGTGCTTAGT/Thiol C6 SS 3′).[40] The system is powered by a circuit chip and directly transmits data to the computer interface, as shown in Fig. 6a and b. The microcontroller unit (MCU) regulates the

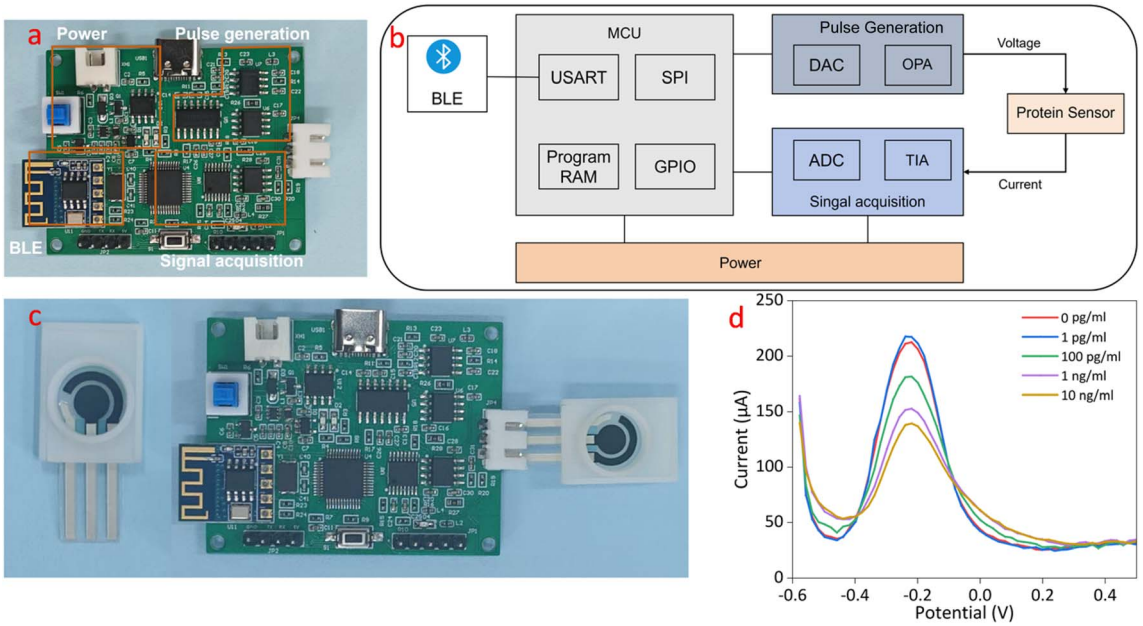

Fig. 6 The composition and the measured outcomes of detecting the IL-6 content with the circuit board. (a) The constitution of the circuit modules on the PCB. (b) The detailed contents of the circuit module system. (c) Schematic diagram of the integrated test for the assembly of electrodes, 3D printed enclosures, and PCB. (d) The result diagram of detecting IL-6 by using the PCB.

digital-to-analog converter (DAC) through Serial Peripheral Interface (SPI) communication to generate the staircase pulse waveform required for DPV measurements. The processed signal from the operational amplifier (OPA) is subsequently applied between the reference electrode and working electrode. During electrochemical reactions, the current generated at the working electrode is converted to voltage through a trans-impedance amplifier (TIA), facilitating analog-to-digital conversion (ADC) acquisition. After the ADC collects the voltage, it sends the data to the MCU for processing, and then sends it to the mobile phone or computer *via* Bluetooth. A dedicated power module ensures stable system operation through optimized power management. Fig. 6c shows the assembly of the sensor and the PCB, which enables portable one-step detection.

To evaluate circuit functionality and improve signal stability, 20 mM potassium ferricyanide solution was employed as the electrochemical signal transmission medium. Experimental results (Fig. 6d) validate the system's functional efficacy in IL-6 detection. This integrated platform establishes a technological foundation for next-generation portable biosensors, particularly promising for clinical monitoring and environmental detection applications.

3.5 Exploration of the possibility of sensor detection for other proteins

Nucleic acid aptamer-specific detection should have strong universality, so the experiment also conducted sensitivity detection for another protein molecule, RPB4. The concentrations of RPB4 protein are as follows: 0.1 pg mL^{-1}, 1 pg mL^{-1}, 10 pg mL^{-1}, 100 pg mL^{-1}, 1 ng mL^{-1}, and 10 ng mL^{-1}, with PBS solution as the diluent. Before testing, it is necessary to exclude any interference from PBS on the electrode signals. The specific experimental method is the same as that for detecting HSA. The RPB4-binding aptamer has been modified on both ends with an amine group on the 5′ and a thiol group on the 3′(5′Amino C6/ATACCAGCTTATTCAATTACAGTAGTGAGGGGTCCGTCGTGGG GTAGTTGGGTCGTGGAGATAGTAAGTGC/Thiol C6 SS 3′). After conducting the gradient test, the DPV signal is shown in Fig. 7, it can be observed that when the RPB4 concentration ranges from 0.1 pg mL^{-1} to 1 ng mL^{-1}, the DPV peak current decreases with increasing concentration, and the DPV peak current value shows a linear relationship with the logarithm of the RPB4 concentration, expressed as $I = 16.9 - 6.9 \quad \log \quad C$, where I is in μA and C is in g mL^{-1}, with $R^2 = 0.940$. This also indicates that the sensor has a highly sensitive recognition capability for RPB4 protein and has an extremely low LOD.

The sensitivity detection of RPB4 indicates that the flexible electrochemical aptamer sensors constructed using the aforementioned experimental methods have strong universality. By simply changing the type of modified aptamer, they can be used to detect different proteins, providing insights for the potential expansion of sensors in the future.

3.6 Specificity and reproducibility

Selectivity is also one of the important characteristics of electrochemical sensors, thus further studying the selectivity of sensors through DPV. The specific experiment method is as follows: firstly, add 100 pg per mL IL-6 protein solution to the working electrode surface, conduct DPV scanning to record the current signal. Then, add 10 nM cortisol to the electrode surface, conduct DPV scanning to record the current signal, and finally add 100 pg per mL HSA and conduct DPV scanning to record the current signal, with a reaction combination time of 30 minutes each time. As can be seen from Fig. 8a, the signal rises after adding IL-6 and cortisol (with PBS as the blank control group), and the signal decreases sharply after adding HSA due to specific capture, which reduces the activity on the electrode surface, hinders electron transfer. This demonstrates that the constructed aptamer sensor can show good selectivity for the target substance.

The stability of the sensor is also a crucial factor, and a large signal drift cannot indicate a good sensor. Repetitive tests are conducted on the constructed sensor to observe its signal stability. Four modified electrodes were tested in the same batch, and the average of three repeated measurements was calculated for each group (direct measurement of the signal, without PBS treatment). As can be seen from Fig. 8b, the DPV peak current signals are basically identical, indicating that the constructed aptamer sensor has good reproducibility.

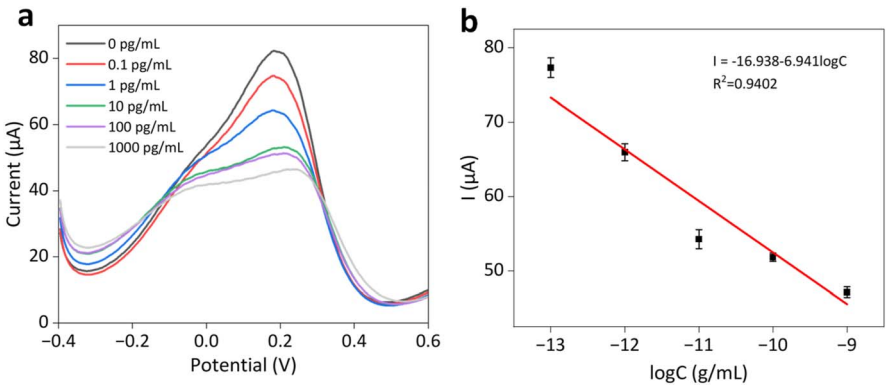

Fig. 7 RPB4 protein sensitivity detection data. (a) DPV curve under different RPB4 protein concentrations. (b) Relationship between the DPV peak current and RPB4 protein concentration after data processing, with the shaded area indicating the error margin.

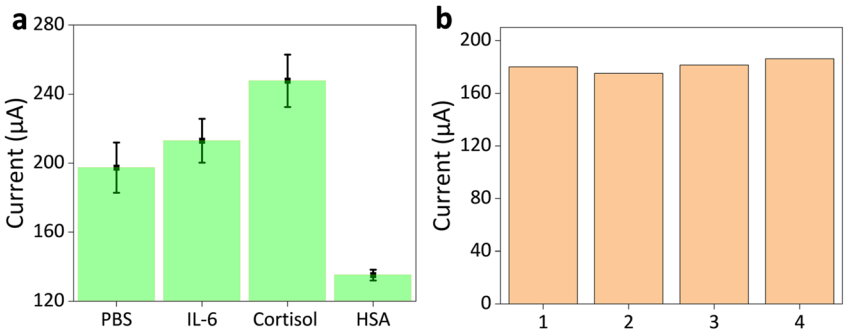

Fig. 8 Selectivity and stability of sensors. (a) Selectivity of sensors. (b) Stability of sensors, the horizontal axis corresponds to the detection sequence.

4 Conclusion

This study presents an electrochemical biosensor leveraging AuNPs to amplify the signal of the PB-based electrode, enabling label-free and ultrasensitive detection of HSA at the femtomolar level. Material characterization *via* SEM and EDS confirmed homogeneous PB and AuNPs electrodeposition on carbon electrodes. CV and EIS validated successful aptamer immobilization and subsequent biorecognition functionality, while MCH effectively passivated nonspecific binding sites on AuNPs surfaces.

The Prussian blue-based aptamer sensor can directly detect in sweat without needing to perform external detection (no need to detect signals in potassium ferricyanide medium), making it more promising for wearable detection of HSA in sweat. The peak current changes *versus* HSA concentration logarithmic relationship diagram reveals a linear correlation between the peak current values and the logarithm of HSA concentration from 0.1 pg mL^{-1} to 1 ng mL^{-1}, with a detection limit of 124 fg mL^{-1} for HSA detection. The sensitivity detection of RBP4 also indicates that this aptamer sensor has universality. The sensor exhibits advantages such as non-invasiveness, miniaturization, portability, and integration. This study anticipates further development into wearable detection devices, and with the extremely low detection limit of the sensor, it is expected to be used for detecting HSA in human body, displaying considerable application potential in future clinical trials.

Author contributions

Conceptualization, Hanghang Cheng, Minghui Yin, Zhi-mei Qi, Ning Xue; methodology, Hanghang Cheng and Chunxiu Liu; validation, Hanghang Cheng, Wentao Chen, Chengyu Zhuang; formal analysis, Minghui Yin; investigation, Minghui Yin, Chengyu Zhuang, Chunxiu Liu; resources, Wentao Chen; data curation, Minghui Yin, Zhi-mei Qi; writing—original draft preparation, Hanghang Cheng, Wentao Chen, Zejun Deng; writing—review and editing, Zejun Deng, Zhi-mei Qi, Chengyu Zhuang, Ning Xue, Chunxiu Liu; visualization, Hanghang Cheng, Wentao Chen; funding acquisition, Ning Xue and Chunxiu Liu. All authors have read and agreed to the published version of the manuscript.

Conflicts of interest

There are no conflicts to declare.

Data availability

The data will be provided upon request to the Lead Contact.

Acknowledgements

This work was supported by the National Key R&D Program of China (No. 2021YFB3200600 and 2020YFC2004500), National Natural Science Foundation of China (No. 62073307, 62273321, 62204243, 62121003, 61931018), CAMS Innovation Fund for Medical Sciences (2019-I2M-5-019), CAS Joint Fund for equipment preresearch and scientific (8091A140106). Lingang Laboratory Research Task (LG-GG-202402-04-01). We would also like to thank Zixuan Song and Lichao Zhang for his/her contributions to the article.

References

1 J. Tu, J. Min, Y. Song, *et al.*, A wireless patch for the monitoring of C-reactive protein in sweat, *Nat. Biomed. Eng.*, 2023, **7**(10), 1293–1306.
2 J. Zhu, L. Zhang, Z. Zhou, *et al.*, Aptamer-based sensing platform using three-way DNA junction-driven strand displacement and its application in DNA logic circuit, *Anal. Chem.*, 2014, **86**(1), 312–316.
3 H. Pei, N. Lu, Y. Wen, *et al.*, A DNA nanostructure-based biomolecular probe carrier platform for electrochemical biosensing, *Adv. Mater.*, 2010, **22**(42), 4754–4758.
4 M. Muratsugu, F. Ohta, Y. Miya, *et al.*, Quartz crystal microbalance for the detection of microgram quantities of human serum albumin: relationship between the frequency change and the mass of protein adsorbed, *Anal. Chem.*, 1993, **65**(20), 2933–2937.
5 Z. Tang, J. Yang, J. Yu, *et al.*, A colorimetric sensor for qualitative discrimination and quantitative detection of volatile amines, *Sensors*, 2010, **10**(7), 6463–6476.
6 M.-C. Chuang, C.-C. Liu and M.-C. Yang, An electrochemical tyrosinase-immobilized biosensor for albumin—toward

a potential total protein measurement, *Sens. Actuators, B*, 2006, **114**(1), 357–363.

7 M. Lin, P. Song, G. Zhou, *et al.*, Electrochemical detection of nucleic acids, proteins, small molecules and cells using a DNA-nanostructure-based universal biosensing platform, *Nat. Protoc.*, 2016, **11**(7), 1244–1263.

8 J. Tu, J. Min and Y. Song, A wireless patch for the monitoring of C-reactive protein in sweat, *Nat. Biomed. Eng.*, 2023, **7**(10), 1293–1306.

9 M. Kessler, A. Meinitzer and O. S. Wolfbeis, Albumin blue 580 fluorescence assay for albumin, *Anal. Biochem.*, 1997, **248**(1), 180–182.

10 V. J. Gauci, E. P. Wright and J. R. Coorssen, Quantitative proteomics: assessing the spectrum of in-gel protein detection methods, *J. Chem. Biol.*, 2011, **4**, 3–29.

11 M.-C. Tu, Y.-T. Chang, Y.-T. Kang, *et al.*, A quantum dot-based optical immunosensor for human serum albumin detection, *Biosens. Bioelectron.*, 2012, **34**(1), 286–290.

12 S. Sang, Y. Li, X. Guo, *et al.*, A portable device for rapid detection of human serum albumin using an immunoglobulin-coating-based magnetoelastic biosensor, *Biosens. Bioelectron.*, 2019, **141**, 111399.

13 W. Gui, X. Chen and Q. Ma, A novel detection method of human serum albumin based on CuInZnS quantum dots-Co^{2+} sensing system, *Anal. Bioanal. Chem.*, 2017, **409**, 3871–3876.

14 M. J. Russo, M. Han, P. E. Desroches, *et al.*, Antifouling strategies for electrochemical biosensing: mechanisms and performance toward point of care based diagnostic applications, *ACS Sens.*, 2021, **6**(4), 1482–1507.

15 M. Cieplak, K. Szwabinska, M. Sosnowska, *et al.*, Selective electrochemical sensing of human serum albumin by semi-covalent molecular imprinting, *Biosens. Bioelectron.*, 2015, **74**, 960–966.

16 B. Wang, C. Zhao, Z. Wang, *et al.*, Wearable aptamer-field-effect transistor sensing system for noninvasive cortisol monitoring, *Sci. Adv.*, 2022, **8**(1), eabk0967.

17 Y. Fan, S. Shi, J. Ma, *et al.*, A paper-based electrochemical immunosensor with reduced graphene oxide/thionine/gold nanoparticles nanocomposites modification for the detection of cancer antigen 125, *Biosens. Bioelectron.*, 2019, **135**, 1–7.

18 A. D. Ellington and J. W. Szostak, In vitro selection of RNA molecules that bind specific ligands, *Nature*, 1990, **346**(6287), 818–822.

19 S. Li, Q. Luo, Y. Liu, *et al.*, Surface molecularly imprinted polymer film with poly(p-aminothiophenol) outer layer coated on gold nanoparticles inner layer for highly sensitive and selective sensing paraoxon, *Polymers*, 2017, **9**(8), 359.

20 K. A. Sarpong, K. Zhang, Y. Luan, *et al.*, Development and application of a novel electrochemical sensor based on AuNPS and difunctional monomer-MIPs for the selective determination of tetrabromobisphenol-S in water samples, *Microchem. J.*, 2020, **154**, 104526.

21 D. Branagan and C. B. Breslin, Electrochemical detection of glucose at physiological pH using gold nanoparticles deposited on carbon nanotubes, *Sens. Actuators, B*, 2019, **282**, 490–499.

22 Y. Shan, J.-J. Xu and H.-Y. Chen, Distance-dependent quenching and enhancing of electrochemiluminescence from a CdS:Mn nanocrystal film by Au nanoparticles for highly sensitive detection of DNA, *Chem. Commun.*, 2009, (8), 905–907.

23 H. Zhao, Y. Yuan, S. Adeloju, *et al.*, Study on the formation of the Prussian blue films on the polypyrrole surface as a potential mediator system for biosensing applications, *Anal. Chim. Acta*, 2002, **472**(1–2), 113–121.

24 C. X. Guo, X. T. Zheng, Z. S. Lu, *et al.*, Biointerface by cell growth on layered graphene–artificial peroxidase–protein nanostructure for in situ quantitative molecular detection, *Adv. Mater.*, 2010, **22**(45), 5164–5167.

25 W. Tang, L. Yin, J. R. Sempionatto, *et al.*, Touch-based stressless cortisol sensing, *Adv. Mater.*, 2021, **33**(18), 2008465.

26 A. Ramanaviciene, N. German, A. Kausaite-Minkstimiene, *et al.*, Glucose biosensor based on dendritic gold nanostructures electrodeposited on graphite electrode by different electrochemical methods, *Chemosensors*, 2021, **9**(8), 188.

27 S. Ghosh, Y. Chen, J. Sebastian, *et al.*, A study on the response of FRET based DNA aptasensors in intracellular environment, *Sci. Rep.*, 2020, **10**(1), 13250.

28 N. Kuntip, D. Japrung and P. Pongprayoon, How human serum albumin-selective DNA aptamer binds to bovine and canine serum albumins, *Biopolymers*, 2021, **112**(3), e23421.

29 M. V. Berezovski, M. Lechmann, M. U. Musheev, *et al.*, Aptamer-facilitated biomarker discovery (AptaBiD), *J. Am. Chem. Soc.*, 2008, **130**(28), 9137–9143.

30 E. E. Ferapontova and K. V. Gothelf, Optimization of the Electrochemical RNA-Aptamer Based Biosensor for Theophylline by Using a Methylene Blue Redox Label, *Electroanalysis*, 2009, **21**(11), 1261–1266.

31 Y. Yang, C. Li, L. Yin, *et al.*, Enhanced charge transfer by gold nanoparticle at DNA modified electrode and its application to label-free DNA detection, *ACS Appl. Mater. Interfaces*, 2014, **6**(10), 7579–7584.

32 M. G. Dastidar, K. Murugappan, D. R. Nisbet, *et al.*, Simultaneous electrochemical detection of glycated and human serum albumin for diabetes management, *Biosens. Bioelectron.*, 2024, **246**, 115876.

33 L. Zhou, G. Figueroa-Miranda, S. Chen, *et al.*, Flexible multielectrode arrays based electrochemical aptasensor for glycated human serum albumin detection, *Sens. Actuators, B*, 2023, **386**, 133730.

34 B. Feyzi-Barnaji, B. Darbasizadeh, E. Arkan, *et al.*, Immunoreaction-triggered diagnostic device using reduced graphene oxide/CuO NPs/chitosan ternary nanocomposite, toward enhanced electrochemical detection of albumin, *J. Electroanal. Chem.*, 2020, **877**, 114642.

35 Z. Shen, S. Ni, W. Yang, *et al.*, Redox probes tagged electrochemical aptasensing device for simultaneous detection of multiple cytokines in real time, *Sens. Actuators, B*, 2021, **336**, 129747.

36 Y. Wu, B. Midinov and R. J. White, Electrochemical aptamer-based sensor for real-time monitoring of insulin, *ACS Sens.*, 2019, **4**(2), 498–503.
37 B. Jiang, F. Li, C. Yang, *et al.*, Aptamer pseudoknot-functionalized electronic sensor for reagentless and single-step detection of immunoglobulin E in human serum, *Anal. Chem.*, 2015, **87**(5), 3094–3098.
38 M. Zhu, C. Xie, F. Xu, *et al.*, Exploring Differential Electron Transfer Kinetics of Electrochemical Aptamer-Based Sensors to Achieve Calibration-Free Measurements, *ACS Sens.*, 2025, **10**(2), 1105–1112.
39 L. Hou, Z. Gao, M. Xu, *et al.*, DNAzyme-functionalized gold–palladium hybrid nanostructures for triple signal amplification of impedimetric immunosensor, *Biosens. Bioelectron.*, 2014, **54**, 365–371.
40 C. Diacci, B. Burtscher, M. Berto, *et al.*, Organic electrochemical transistor aptasensor for interleukin-6 detection, *ACS Appl. Mater. Interfaces*, 2023, **16**(45), 61467–61474.